# Multi-point Explicit Differencing (MED)

# for Time Integrations of the Wave Equation

Celal S. Konor

*Department of Atmospheric Science, Colorado State University,*

*Fort Collins, Colorado*

Akio Arakawa

*Department of Atmospheric and Oceanic Sciences, University of California, Los Angeles,*

*Los Angeles, California*

Accepted for publication by *Monthly Weather Review*

March 2007

---

*Corresponding author address*: Dr. Celal S. Konor, Department of Atmospheric Science, Colorado State University, 200 West Lake Street, Fort Collins, Colorado, 80523-1371.

E-mail: csk@atmos.colostate.edu

## Abstract

For time integrations of the wave equation, it is desirable to use a scheme that is stable over a wide range of the Courant number. Implicit schemes are examples of such schemes, but they do that job at the expense of global calculation, which becomes an increasingly serious burden as the horizontal resolution becomes higher while covering a large horizontal domain. If we look at what an implicit scheme does from the point of view of explicit differencing, it is a multi-point scheme that requires information at all grid points in space. Physically this is an over-demanding requirement since wave propagation in the real atmosphere has a finite speed.

The purpose of this study is to seek the feasibility of constructing an explicit scheme that does essentially the same job as an implicit scheme with a finite number of grid points in space. In this paper, we use a space-centered trapezoidal implicit scheme as the target scheme as an example. We show that an explicit space-centered scheme with the forward time differencing using an infinite number of grid points in space can be made equivalent to the trapezoidal implicit scheme. To avoid global calculation, we then introduce a truncated version of the scheme that uses only a finite number of grid points while maintaining the stability. We call this approach of constructing a stable explicit scheme "Multi-point Explicit Differencing (MED)". We show that the coefficients in a MED scheme can be numerically determined by single-time-step integrations of the target scheme. With this procedure, it is rather straightforward to construct a MED scheme for an arbitrarily-shaped grid and/or boundaries.

In a MED scheme, the number of grid points necessary to maintain stability and, therefore, the CPU time needed for each time step increase as the Courant number increases. Due to this overhead, the MED scheme with a large time step can be more efficient than a usual explicit scheme with a smaller time step only for complex multi-level models with detailed physics. The efficiency of a MED scheme also depends on how the advantage of parallel computing is taken.

## 1. Introduction

Selection of a time-integration scheme is one of the most fundamental issues in the development of an atmospheric model. In particular, the constraint on the length of time step required for computational stability can be a serious burden to the economy of the model, especially when the model is complex so that lengthy calculations are needed for each time step. For explicit time-differencing schemes applied to the wave or advection equation, the constraint is such that the Courant number for the fastest wave propagation must not exceed the order of one. The alternative is the use of an implicit scheme (or a semi-implicit scheme in which an implicit scheme is partially applied) that is stable for arbitrarily large values of the Courant number.

The implicit time-integration schemes achieve stability at the expense of global calculation, in which information from all grid points is used at each time step. Thus the use of an implicit scheme remains computationally advantageous only when the gain due to the use of a longer time step supersedes the loss due to the computational burden of global calculation. It has been known that, for the conventional resolution of global models, semi-implicit schemes provide better computational efficiency, especially in the spectral models with global basis functions. The reviews of these schemes and examples of their applications to various models can be found in Kurihara (1965), Holton (1967), Kwizak and Robert (1971), Robert et al. (1972), Bourke (1974), Burridge (1975), Tapp and White (1976), Simmons et al. (1978), Cullen (1990), Tanguay et al. (1990), Purser and Leslie (1994) and Yeh et al. (2002). A hybrid implicit/semi-Lagrangian scheme is also proposed by Israeli et al. (2000).

As the horizontal resolution of a model using an implicit scheme becomes higher, however, the computational burden due to global calculation becomes increasingly serious, particularly in view of parallel computing. The efficiency of an implicit scheme is closely related to the efficiency of the elliptic solver used in the integration, which is commonly based on the multigrid method (Brandt, 1977; Fulton et al., 1986; and Briggs et al., 2000). While this method is easily applicable and computationally economical for problems with regular boundaries, its generalization to handle arbitrarily-shaped grids and/or boundaries can be extremely complicated. Under these circumstances, it is not straightforward to assess the merit of an implicit scheme over the explicit schemes.

There are studies, which propose explicit schemes as an alternative to the implicit ones that are stable for longer time steps than the traditional stability criteria require. Two noticeable examples of this approach are Verwer (1996) and Eriksson et al. (2003). In these examples, the equations are first discretized spatially using a fixed number of grid points in space and then a multi-level time integration scheme is applied to stabilize solution for a desired large time-step. In Eriksson et al. (2003), the multi-level scheme involves in a few stabilizing small time steps and a large time step, in which the length and number of small time steps are automatically adjusted to maintain stability for the desired large time step. However, these schemes are designed for the solutions of equations, in which decay or dissipative effects are dominant. Here we address a completely different problem: the propagation of waves with no or little dissipative effects. Frank et al. (2005) proposes a staggered time integration scheme combined with a "regularization" of the continuous momentum equation to satisfy a neutral stability criterion for large Courant numbers with

respect to wave. However, this method does not eliminate the global calculations because the "regularization" requires solution of an elliptic equation.

In this study, we seek the feasibility of constructing an explicit scheme that does essentially the same job as an implicit scheme but with a finite number of grid points in space. Any explicit scheme that does the same job as an implicit scheme must inevitably use a multi-point space differencing to maintain stability for large time steps. This can be illustrated considering the following one-dimensional linear equation for a component propagating in the x direction:

$$\frac{\partial \Psi}{\partial t} + c\frac{\partial \Psi}{\partial x} = 0 , \qquad (1)$$

where $\Psi$ is an arbitrary quantity associated with the component and c is the propagation speed. Consider an Eulerian finite-difference scheme applied to the point on the x-t plane shown by the large solid dot in Fig.1. Here the horizontal and vertical lines show time levels and grid points in space, respectively, $\Delta t$ and $\Delta x$ are the time interval and the grid size, respectively. It is clear that the solution of the continuous equation (1) at the small solid dot is given by the value at the open dot, which is the intersection of the characteristics $x - ct = \text{const.}$ shown by the dashed line with the line representing the initial time. For an Eulerian discrete system to recognize this value with a stable algorithm (i.e., basically interpolation rather than extrapolation) for an arbitrary Courant number $\mu \equiv c\Delta t/\Delta x$, it is obvious that multiple grid points are needed for space differencing. We further note that, since c is finite, the number of grid points can be finite, whereas an implicit scheme requires information at an infinite number of grid points unless the domain is bounded or periodic as is the case for the global atmosphere. As the horizontal resolution increases, however, this

advantage due to the existence of a boundary or periodicity tends to vanish since a larger and larger number of grid points are needed to cover the entire globe.

Section 2 presents the linearized shallow-water equations and the corresponding wave equation in their continuous form. Sections 3 and 4 illustrate how an explicit scheme that mimics the trapezoidal implicit scheme can be constructed using a rectangular grid. Section 3 presents the trapezoidal implicit scheme with the simplest centered space differencing for the linearized shallow-water equations. Section 4 introduces MED schemes based on multi-point horizontal differencing with the forward time differencing. Section 4 then shows that a member of the MED schemes can be made equivalent to the trapezoidal implicit scheme presented in section 3. We call this scheme "equivalent trapezoidal (ETZ) scheme". Section 4 also introduces "truncated equivalent trapezoidal (TETZ) scheme", in which only a finite number of grid points are used, and discusses its stability. Section 5 presents a numerical method to construct a TETZ scheme applicable to any grid. Section 6 discusses the implementation of the TETZ scheme in the nonlinear shallow-water equations on a square grid and demonstrates its performance in numerical simulation of gravity-wave propagations in regularly- and arbitrarily-shaped domains. Finally, section 7 presents summary and conclusions.

**2. Linearized shallow-water equations**

For the purpose of later use in this paper, here we present the linearized shallow-water equations with no basic current and no Coriolis force, and the corresponding wave equation. The linearized continuity and divergence equations are given by

$$\frac{\partial h}{\partial t} = -H\delta \qquad (2a)$$

and

$$\frac{\partial \delta}{\partial t} = -g\nabla^2 h, \tag{2b}$$

where h and H are the perturbation and mean height of the free surface, respectively, $\delta$ is the divergence given by $\nabla \cdot \mathbf{v}$, where $\mathbf{v}$ is the horizontal velocity, and g is the gravitational acceleration. For this system, the velocity potential $\chi$ and the divergent component of the velocity can be obtained from $\nabla^2 \chi = \delta$ and $\mathbf{v} = \nabla \chi$, respectively. The wave equation for h can be derived by eliminating the divergence between (2a) and (2b) as

$$\frac{\partial^2 h}{\partial t^2} = c^2 \nabla^2 h, \tag{3}$$

where c is the propagation speed of the waves given by $c \equiv \sqrt{gH}$.

## 3. Discretization of the linearized shallow-water equations with the trapezoidal implicit time integration scheme

Here we present a discrete version of (2a) and (2b) with the trapezoidal implicit scheme in time and the simplest centered scheme in space on a rectangular grid shown in Fig. 2. The discrete continuity and divergence equations are

$$\frac{h_{i,j}^{(n+1)} - h_{i,j}^{(n)}}{\Delta t} = -\frac{H}{2}\left[\delta_{i,j}^{(n+1)} + \delta_{i,j}^{(n)}\right] \tag{4a}$$

and

$$\frac{\delta_{i,j}^{(n+1)} - \delta_{i,j}^{(n)}}{\Delta t} = -\frac{g}{2}\left[\left(\tilde{\nabla}^2 h\right)_{i,j}^{(n+1)} + \left(\tilde{\nabla}^2 h\right)_{i,j}^{(n)}\right], \tag{4b}$$

respectively. Here the superscript denotes a time level, i and j are horizontal integer indices for the grid points increasing with x and y, respectively. In (4b), the discrete Laplacian operator is defined as

$$\left(\tilde{\nabla}^2 h\right)_{i,j} \equiv \frac{1}{(\Delta x)^2}\left(h_{i+1,j} - h_{i-1,j} - 2h_{i,j}\right) + \frac{1}{(\Delta y)^2}\left(h_{i,j+1} - h_{i,j-1} - 2h_{i,j}\right). \qquad (4c)$$

From (4a) and (4b), we can derive the discrete version of the wave equation (3) given by

$$\frac{h_{i,j}^{(n+1)} - 2h_{i,j}^{(n)} + h_{i,j}^{(n-1)}}{(\Delta t)^2} = \frac{gH}{4}\left[\left(\tilde{\nabla}^2 h\right)_{i,j}^{(n+1)} + 2\left(\tilde{\nabla}^2 h\right)_{i,j}^{(n)} + \left(\tilde{\nabla}^2 h\right)_{i,j}^{(n-1)}\right]. \qquad (5)$$

We now analyze the normal modes of the discrete system given by (4a) and (4b) seeking the solutions in the form

$$\left.\begin{aligned} h_{i,j}^{(n)} &\equiv \mathrm{Re}\left[\hat{h}^{(n)} e^{i(k\Delta x i + \ell \Delta y j)}\right] \\ \delta_{i,j}^{(n)} &\equiv \mathrm{Re}\left[\hat{\delta}^{(n)} e^{i(k\Delta x i + \ell \Delta y j)}\right] \end{aligned}\right\}, \qquad (6)$$

where $\hat{h}^{(n)}$ and $\hat{\delta}^{(n)}$ are the complex amplitudes of h and $\delta$ at time level n, respectively, $i = \sqrt{-1}$, and k and $\ell$ are the wavenumbers in x and y directions, respectively. Substituting (6) into (4a) and (4b) with (4c) and then eliminating $\hat{\delta}^{(n+1)}$ between the continuity and divergence equations, we obtain the equations that predicts the complex amplitudes of the wave as

$$\hat{h}^{(n+1)} = 4F(\xi,\eta)\hat{h}^{(n)} - 4G(\xi,\eta)H\Delta t\hat{\delta}^{(n)} \qquad (7a)$$

and

$$H\Delta t\hat{\delta}^{(n+1)} = 4F(\xi,\eta)\hat{\delta}^{(n)} + 16\mu^{*2}G(\xi,\eta)\hat{h}^{(n)}, \qquad (7b)$$

respectively. In (7a) and (7b), we have used the definitions

$$F(\xi,\eta) \equiv \frac{1}{4}\frac{1-\mu^{*2}}{1+\mu^{*2}} \quad \text{and} \quad G(\xi,\eta) \equiv \frac{1}{4}\frac{1}{1+\mu^{*2}}, \qquad (8)$$

where

$$\mu^{*2} \equiv \mu_x^2 \sin^2(\xi/2) + \mu_y^2 \sin^2(\eta/2), \tag{9a}$$

$\xi \equiv k\Delta x$ and $\eta \equiv \ell\Delta y$, and the Courant number in x and y directions are defined by

$$\left.\begin{aligned} \mu_x &\equiv \sqrt{gH}\,\Delta t/\Delta x \\ \mu_y &\equiv \sqrt{gH}\,\Delta t/\Delta y \end{aligned}\right\}, \tag{9b}$$

respectively. If we let $\hat{h}^{(n+1)} = \lambda\hat{h}^{(n)}$ and $\hat{\delta}^{(n+1)} = \lambda\hat{\delta}^{(n)}$, where $\lambda$ is the complex amplification factor of a normal mode, (7a) and (7b) with (8) yield

$$\left[\lambda - 4F(\xi,\eta)\right]\hat{h}^{(n)} + 4G(\xi,\eta)H\Delta t\hat{\delta}^{(n)} = 0 \tag{10a}$$

and

$$16\mu^{*2}G(\xi,\eta)\hat{h}^{(n)} - \left[\lambda - 4F(\xi,\eta)\right]H\Delta t\hat{\delta}^{(n)} = 0, \tag{10b}$$

respectively. For non-trivial solutions of (10a) and (10b), the amplification factor $\lambda$ must satisfy

$$\lambda^2 - 8F(\xi,\eta)\lambda + \left[4F(\xi,\eta)\right]^2 + \left[8\mu^* G(\xi,\eta)\right]^2 = 0 \tag{11}$$

and thus

$$\lambda = 4F(\xi,\eta) \pm i\left[8\mu^* G(\xi,\eta)\right], \tag{12}$$

where F and G are given by (8). Since the amplification factor $\lambda$ has an imaginary part and $|\lambda|^2 = 1$, the solution is a progressive neutral wave.

## 4. Discretization of the linearized shallow-water equations with MED

Our motivation in this paper is to construct an explicit scheme that mimic the trapezoidal implicit scheme. As discussed in the introduction, multi-point space differencing is needed to accomplish this task. Below we start with introduction of multi-point averaging,

which is the essential part of the scheme to be constructed. Then, a family of MED schemes are discussed using a rectangular grid as an example.

*a. Two-dimensional multi-point averaging*

Let $\Psi$ be an arbitrary variable. We express the two-dimensional multi-point weighted averaging of $\Psi$ applied to the target grid point (i , j) by

$$\left[\mathbf{A}(\Psi)\right]_{i,j} \equiv \sum_{i'=-J}^{J}\sum_{j'=-J}^{J} a_{i',j'}\Psi_{i+i',j+j'}\,, \tag{13}$$

where $\mathbf{A}$ is an averaging operator and $a_{i',j'}$ is a weighting coefficient satisfying

$$\sum_{i'=-J}^{J}\sum_{j'=-J}^{J} a_{i',j'} = 1\,. \tag{14a}$$

For symmetric averaging, we have

$$a_{i',j'} = a_{-i',j'}\,,\quad a_{i',j'} = a_{i',-j'}\quad \text{and}\quad a_{i',j'} = a_{-i',-j'}\,. \tag{14b}$$

The averaging is performed over the "domain of dependence" from i'= –J to +J and j'= –J to j'= +J. Using (14a) in (13), we can obtain an alternative expression for the multi-point averaging as

$$\begin{aligned}\left[\mathbf{A}(\Psi)\right]_{i,j} \equiv a_{0,0}\Psi_{i,j} &+ \sum_{i'=1}^{J} a_{i',0}\left(\Psi_{i+i',j} + \Psi_{i-i',j}\right) + \sum_{j'=1}^{J} a_{0,j'}\left(\Psi_{i,j+j'} + \Psi_{i,j-j'}\right) \\ &+ \sum_{i'=1}^{J}\sum_{j'=1}^{J} a_{i',j'}\left(\Psi_{i+i',j+j'} + \Psi_{i-i',j-j'} + \Psi_{i+i',j-j'} + \Psi_{i-i',j+j'}\right).\end{aligned} \tag{15}$$

Since the operator $\mathbf{A}$ is independent of i and j, the multi-point finite difference Laplacian satisfies

$$\left[\mathbf{A}\left(\tilde{\nabla}^2\psi\right)\right]_{i,j} = \left[\tilde{\nabla}^2\mathbf{A}(\psi)\right]_{i,j}, \tag{16}$$

where $\tilde{\nabla}^2$ is defined by (4c).

*b. An explicit scheme based on multi-point averaging*

Expecting that a MED scheme based on the multi-point averaging described above can be made equivalent to the trapezoidal implicit scheme, we first write the discrete continuity and divergence equations as

$$h_{i,j}^{(n+1)} = \left[\mathbf{C}\left(h^{(n)}\right)\right]_{i,j} - H\Delta t\left[\mathbf{A}\left(\delta^{(n)}\right)\right]_{i,j} \tag{17a}$$

and

$$\delta_{i,j}^{(n+1)} = \left[\mathbf{C}\left(\delta^{(n)}\right)\right]_{i,j} - g\Delta t\left[\tilde{\nabla}^2\mathbf{A}\left(h^{(n)}\right)\right]_{i,j}, \tag{17b}$$

respectively, where **C** is another multi-point averaging operator. In (17b), (16) has been used. To examine the stability of the solution of (17a) and (17b), we first use (6) in $\left[\mathbf{C}\left(\psi^{(n)}\right)\right]_{i,j}$ and $\left[\mathbf{A}\left(\psi^{(n)}\right)\right]_{i,j}$, where $\psi$ is either h or $\delta$, to obtain

$$\left.\begin{aligned}\mathbf{C}\left(\hat{\Psi}^{(n)}e^{i(\xi i+\eta j)}\right) &\equiv 4\tilde{F}(\xi,\eta)\hat{\Psi}^{(n)}\\ \mathbf{A}\left(\hat{\Psi}^{(n)}e^{i(\xi i+\eta j)}\right) &\equiv 4\tilde{G}(\xi,\eta)\hat{\Psi}^{(n)}\end{aligned}\right\}. \tag{18}$$

Using (15) and a similar expression for the operator **C**, we find that $\tilde{F}$ and $\tilde{G}$ in (18) can be expressed as

$$\left.\begin{aligned}\tilde{F}(\xi,\eta) &\equiv \frac{c_{0,0}}{4} + \frac{1}{2}\sum_{i'=1}^{J} c_{i',0}\cos(\xi i') + \frac{1}{2}\sum_{j'=1}^{J} c_{0,j'}\cos(\eta j') + \sum_{i'=1}^{J}\sum_{j'=1}^{J} c_{i',j'}\cos(\xi i')\cos(\eta j')\\ \tilde{G}(\xi,\eta) &\equiv \frac{a_{0,0}}{4} + \frac{1}{2}\sum_{i'=1}^{J} a_{i',0}\cos(\xi i') + \frac{1}{2}\sum_{j'=1}^{J} a_{0,j'}\cos(\eta j') + \sum_{i'=1}^{J}\sum_{j'=1}^{J} a_{i',j'}\cos(\xi i')\cos(\eta j')\end{aligned}\right\}. \tag{19}$$

In (19), $c_{i',j'}$ and $a_{i',j'}$ are weighting coefficients to be determined while satisfying (14a) with (14b). Then, using (6) and (18), we can rewrite (17a) and (17b) as

$$\hat{h}^{(n+1)} = 4\tilde{F}(\xi,\eta)\hat{h}^{(n)} - 4\tilde{G}(\xi,\eta)H\Delta t\hat{\delta}^{(n)} \tag{20a}$$

and

$$H\Delta t\hat{\delta}^{(n+1)} = 4\tilde{F}(\xi,\eta)H\Delta t\hat{\delta}^{(n)} + 16\mu^{*2}\tilde{G}(\xi,\eta)\hat{h}^{(n)}. \tag{20b}$$

These equations are similar to (7a) and (7b) for the trapezoidal scheme but now $\tilde{F}(\xi,\eta)$ and $\tilde{G}(\xi,\eta)$ are given by (19) instead of (8).

Following a procedure similar to the derivation of (12), we find the expression for the amplification factor for the MED scheme as

$$\lambda = 4\tilde{F}(\xi,\eta) \pm i\left[8\mu^{*}\tilde{G}(\xi,\eta)\right]. \tag{21}$$

For the solution to be stable,

$$|\lambda|^2 = \left[4\tilde{F}(\xi,\eta)\right]^2 + \left[8\mu^{*}\tilde{G}(\xi,\eta)\right]^2 \le 1 \tag{22}$$

must be maintained.

*c. Equivalent trapezoidal (ETZ) scheme*

In this subsection, we present a procedure to determine the coefficients $a_{i',j'}$ and $c_{i',j'}$ in such a way that the explicit scheme given by (17a) and (17b) is equivalent to the trapezoidal implicit scheme given by (7a) and (7b). For this purpose, we require that (20a) and (20b) share the same $\hat{h}^{(n+1)}$ and $\hat{\delta}^{(n+1)}$ with (7a) and (7b), respectively, from the same initial condition, $\hat{h}^{(n)}$ and $\hat{\delta}^{(n)}$. This can be achieved by choosing

$$\tilde{F}(\xi,\eta) = F(\xi,\eta) \quad \text{and} \quad \tilde{G}(\xi,\eta) = G(\xi,\eta). \tag{23}$$

Then, in view of (19), $c_{i',j'}$ and $a_{i',j'}$ are the coefficients in the cosine Fourier expansion of the functions $F(\xi,\eta)$ and $G(\xi,\eta)$ given by (8), respectively. We calculate the coefficients $c_{i',j'}$ and $a_{i',j'}$ with a sufficiently large value of J (=250) so that the approximate series given by $\tilde{F}$ and $\tilde{G}$ are virtually identical to F and G, respectively. The sum of $c_{i',j'}$ and $a_{i',j'}$ between $-250 \le i' \le 250$ and $-250 \le j' \le 250$ are approximately unity, automatically satisfying (14a). We present the coefficients obtained in this way in Fig. 3 for $j'=0$ and selected values of $\mu$. In the figure, we see that the coefficients $a_{i',0}$ monotonically and rapidly decrease away from the target point ($i'=0$) and finally become negligible for all Courant numbers. The coefficients $c_{i',0}$ start with a minimum value at the target point ($i'=0$), negative for the Courant numbers larger than one, then become positive and maximum at the surrounding grid points ($i'=1$ and $i'=-1$), and then monotonically and rapidly decrease away from the those points. The negative weighting of $c_{0,0}$ for the Courant numbers larger than one indicates that the contribution of the target point to the averaging is through an extrapolation.

In conclusion, the scheme given by (17a) and (17b) is equivalent to the trapezoidal scheme discussed in section 3 if the coefficients given by (23) are used. Fig. 3 presents examples of such coefficients. We call this scheme "equivalent trapezoidal (ETZ) scheme".

*d. Truncated equivalent trapezoidal (TETZ) scheme*

The equivalent trapezoidal scheme presented in the last subsection is an explicit scheme but it behaves as the implicit trapezoidal scheme does. This is achieved by using information from practically all grid points in the domain because the scheme uses a very

large J. As stated earlier, our objective is to construct explicit schemes that do essentially the same job as the implicit trapezoidal scheme but using a finite number of grid points. Here we present "truncated equivalent trapezoidal (TETZ) scheme", which accomplishes this task. The prospect for such a scheme can be seen, for example, in the distribution of the coefficients $a_{i',0}$ and $c_{i',0}$ in Fig. 3, which shows that the coefficients become negligible at grid points sufficiently far from the target point.

In truncating the coefficients, we are guided by the stability analysis presented in subsection 4*b*. We first define $\tilde{F}_T(\xi,\eta)$ and $\tilde{G}_T(\xi,\eta)$ in a way similar to (19) but with the coefficients $\tilde{a}_{i',j'}$ and $\tilde{c}_{i',j'}$ truncated at a finite J and renormalized so that their sums over $-J \le i' \le J$ and $-J \le j' \le J$ are unity. The criterion for neutral solutions ($|\lambda|^2 = 1$) obtained from (22) but applied to the truncated system is satisfied if we choose

$$\tilde{F}_T(\xi,\eta) = \begin{cases} \dfrac{1}{4}\left\{1-\left[8\mu^*\tilde{G}_T(\xi,\eta)\right]^2\right\}^{1/2} & \text{for} \quad \mu^*(\xi,\eta) \le 0 \\ -\dfrac{1}{4}\left\{1-\left[8\mu^*\tilde{G}_T(\xi,\eta)\right]^2\right\}^{1/2} & \text{for} \quad \mu^*(\xi,\eta) > 0 \end{cases} . \qquad (24a)$$

In choosing the signs in (24a), we are guided by the definition of F given by (8). With this choice of $\tilde{F}_T(\xi,\eta)$, the stability criterion is reduced to

$$1-\left[8\mu^*\tilde{G}_T(\xi,\eta)\right]^2 \ge 0 . \qquad (24b)$$

The first step of the truncation and renormalization process is to find the minimum J for a given Courant number $\mu$ that satisfies (24b) while maintaining

$$\tilde{a}_{0,0} + 2\sum_{i'=1}^{J}\tilde{a}_{i',0} + 2\sum_{j'=1}^{J}\tilde{a}_{0,j'} + 4\sum_{i'=1}^{J}\sum_{j'=1}^{J}\tilde{a}_{i',j'} = 1 . \qquad (25)$$

To find the coefficients in (25), we use a least-square method, which minimizes the mean-square error between the continuous function G given by (8) and its approximation $\tilde{G}_T$, which is a truncated version of $\tilde{G}$ given by (19), for the intervals $-\pi \le \xi \le \pi$ and $-\pi \le \eta \le \pi$. Thus we let

$$\int_{-\pi}^{\pi}\int_{-\pi}^{\pi}\left[\tilde{G}_T(\xi,\eta) - G(\xi,\eta)\right]^2 d\eta d\xi \to \text{minimum}, \tag{26}$$

which yields

$$\int_{-\pi}^{\pi}\int_{-\pi}^{\pi}\left[\tilde{G}_T - G\right]\left[\frac{\partial \tilde{G}_T}{\partial \tilde{a}_{0,0}}\frac{\partial \tilde{a}_{0,0}}{\partial \tilde{a}_{i',j'}} + \frac{\partial \tilde{G}_T}{\partial \tilde{a}_{i',j'}}\right] d\xi\, d\eta = 0. \tag{27}$$

To derive (27), we treat $\tilde{a}_{0,0}$ is a function of the rest of the coefficients as suggested by (25). From (19) and (25), we obtain $\partial \tilde{G}_T / \partial \tilde{a}_{0,0} = 1/4$, $\partial \tilde{G}_T / \partial \tilde{a}_{i',j'} = \cos(\xi i')\cos(\eta j')$ and $\partial \tilde{a}_{0,0} / \partial \tilde{a}_{i',j'} = -4$. Using these relations, $\int_{-\pi}^{\pi}\int_{-\pi}^{\pi} \tilde{G}_T\, d\xi\, d\eta = \pi^2 \tilde{a}_{0,0}$ and $\int_{-\pi}^{\pi}\int_{-\pi}^{\pi} \tilde{G}_T \cos(\xi i')\cos(\eta j')\, d\xi\, d\eta = \pi^2 \tilde{a}_{i',j'}$ in (27), we obtain

$$\tilde{a}_{i',j'} = \tilde{a}_{0,0} - \frac{1}{\pi^2}\int_{-\pi}^{\pi}\int_{-\pi}^{\pi} G\left[1 - \cos(\xi i')\cos(\eta j')\right] d\xi\, d\eta \tag{28a}$$

and, similarly,

$$\tilde{a}_{i',0} = \tilde{a}_{0,0} - \frac{1}{\pi^2}\int_{-\pi}^{\pi}\int_{-\pi}^{\pi} G\left[1 - \cos(\xi i')\right] d\eta d\xi \tag{28b}$$

and

$$\tilde{a}_{0,j'} = \tilde{a}_{0,0} - \frac{1}{\pi^2}\int_{-\pi}^{\pi}\int_{-\pi}^{\pi} G\left[1 - \cos(\eta j')\right] d\eta d\xi. \tag{28c}$$

Note that, in (28a) to (28c), G is given by (8). Finally, $\tilde{a}_{0,0}$ is obtained by using (28a)-(28c) in (25).

To study the stability of the truncated system, we first obtain the coefficient $\tilde{a}_{i',j'}$ from (28a-c) and (25) for different J's for a given Courant number $\mu$. Then we calculate $\left(8\mu^*\tilde{G}_T\right)^2_{max} \equiv \text{Max}\left\{\left[8\mu^*\tilde{G}_T(\xi,\eta)\right]^2\right\}$ in the interval of $-\pi \le \xi \le \pi$ and $-\pi \le \eta \le \pi$. Recall that the stability criterion given by (24b) requires $\left(8\mu^*\tilde{G}_T\right)^2_{max} \le 1$. Fig. 4 illustrates $\left(8\mu^*\tilde{G}_T\right)^2_{max}$ as a function of J for selected Courant numbers. The figure shows that $\left(8\mu^*\tilde{G}_T\right)^2_{max}$ asymptotically approaches to unity from above as J increases. Since the stability is gradually reached with increasing J, we tabulate the minimum J's that keep $\left(8\mu^*\tilde{G}_T\right)^2_{max}$ under 1.05 and 1.01 for the Courant numbers between 1 and 10 in Table 1. In practice, we use $\left(8\mu^*\tilde{G}_T\right)^2_{max} \le 1.01$ as the stability limit and the corresponding minimum J's in the truncation process. In Table 2, we show the truncated weighting coefficient $\tilde{a}_{i',j'}$ obtained with J given in the lower panel of Table 1. Using a similar procedure, we find the truncated weighting coefficient $\tilde{c}_{i',j'}$. The coefficients obtained in this way are tabulated in Table 3 for the Courant numbers presented in Table 2. Although not shown, these coefficients are virtually identical to those for the ETZ scheme. As expected, this implies that the truncation does not substantially modify the coefficients.

In summary, we have shown that a scheme stable for a wide range of the Courant number can be constructed for a rectangular grid following the MED approach, in which the coefficients in the scheme are analytically determined. For an irregular grid, however, we

must find a more general method to construct a MED scheme that is applicable to any grid. This problem is discussed in the next section.

## 5. TETZ scheme for an arbitrary grid

To develop a TETZ scheme for a more general model, we present in this section an algorithm to numerically determine the weighting coefficients for an arbitrary grid. The algorithm assumes that a discrete linearized shallow-water equation model with the trapezoidal implicit scheme is available and uses the results of single-step integrations of the model starting from a selected set of initial conditions. It then finds the coefficients of a MED scheme that produces identical results to those obtained by the trapezoidal scheme from the same set of initial conditions.

To perform the one-step integrations, the implicit trapezoidal scheme given by (4a) and (4b) is manipulated to the form

$$\left(\tilde{\nabla}^2 h\right)_j^{(n+1)} - m^2 h_j^{(n+1)} = -\left(\tilde{\nabla}^2 h\right)_j^{(n)} - m^2 h_j^{(n)} + m^2 H\Delta t \delta_j^{(n)}, \qquad (29a)$$

where $m^2 \equiv 4\Big/\left[gH(\Delta t)^2\right]$ and $\tilde{\nabla}^2$ is the discrete Laplacian defined for the grid used, and

$$\delta_j^{(n+1)} = -\delta_j^{(n)} - \frac{2}{H\Delta t}\left[h_j^{(n+1)} - h_j^{(n)}\right], \qquad (29b)$$

respectively. In (29a) and (29b), we use a single index j to identify the grid points on the 2D domain. The MED scheme for the shallow-water equations given by (17a) and (17b) are also generalized to an arbitrary grid as

$$h_j^{(n+1)} = \sum_{j'}^{J} c_{j,j'} h_{j+j'}^{(n)} - H\Delta t \sum_{j'}^{J} a_{j,j'} \delta_{j+j'}^{(n)} \qquad (30a)$$

and

$$\delta_j^{(n+1)} = \sum_{j'}^{J} c_{j,j'} \delta_{j+j'}^{(n)} - g\Delta t \sum_{j'}^{J} a_{j,j'} \left( \tilde{\nabla}^2 h^{(n)} \right)_{j+j'}, \tag{30b}$$

where j and $j+j'$ denote a target grid point at which predictions are made and an arbitrary grid point surrounding the target point, respectively, while J denotes the number of all grid points used in the scheme, the determination of which will be discussed later. While the scheme is required to be identical to the ETZ and TETZ schemes for a very large J and a finite J, respectively. For consistency, the weighting coefficients must satisfy

$$\sum_{j'}^{J} a_{j,j'} = \sum_{j'}^{J} c_{j,j'} = 1. \tag{31}$$

To find the coefficients for the target point located at $j = j_0$, we use the following initial condition:

$$h_j^{(0)} = 0 \qquad \text{for all } j \tag{32a}$$

$$\delta_j^{(0)} = \begin{cases} 1/\sigma_{j_0} & \text{for } j = j_0 \\ -1/\sigma_{j_0+j'} & \text{for } j = j_0 + j' \\ 0 & \text{for } j \neq j_0, j_0 + j' \end{cases} \tag{32b}$$

on a grid shown in Fig. 5. In (32a) and (32b), $\sigma$ is the area of the grid cell represented by the grid point. Note that the initial condition satisfies $\sum_j \delta_j^{(0)} \sigma_j = 0$, where the sum is taken over the entire domain. This particular initial condition is selected because it provides a relatively simple way of determining the coefficients for the TETZ scheme as described below.

After the single-step integration of the implicit scheme given by (29a) and (29b), we obtain $h_j^{(1)}$ and $\delta_j^{(1)}$, which are predicted values of h and $\delta$ at the grid point j. We now require that the TETZ scheme given by (30a) and (30b) produce identical values of $h_j^{(1)}$ and

$\delta_j^{(1)}$ with the same initial condition. Using the values obtained by the implicit scheme and the initial condition given by (32a) and (32b) in (30a) and (30b) for given $j_0$ and $j'$, we obtain

$$\frac{a_{j_0,j'}}{\sigma_{j_0+j'}} = \frac{a_{j_0,0}}{\sigma_{j_0}} + \frac{1}{H\Delta t} h_{j_0}^{(1)} \tag{33a}$$

and

$$\frac{c_{j_0,j'}}{\sigma_{j_0+j'}} = \frac{c_{j_0,0}}{\sigma_{j_0}} - \delta_{j_0}^{(1)}, \tag{33b}$$

respectively. We repeat this procedure for all possible $j'$ while still fixing $j_0$. To determine $a_{j_0,0}$ and $c_{j_0,0}$, we write $\sum_{j'\neq 0}^{J} (33a)\sigma_{j_0+j'}$ and $\sum_{j'\neq 0}^{J} (33b)\sigma_{j_0+j'}$ as

$$\sum_{j'\neq 0}^{J} a_{j_0,j'} = \frac{a_{j_0,0}}{\sigma_{j_0}} \sum_{j'\neq 0}^{J} \sigma_{j_0+j'} + \frac{1}{H\Delta t} \sum_{j'\neq 0}^{J} h_{j_0}^{(1)} \sigma_{j_0+j'} \tag{34a}$$

and

$$\sum_{j'\neq 0}^{J} c_{j_0,j'} = \frac{c_{j_0,0}}{\sigma_{j_0}} \sum_{j'\neq 0}^{J} \sigma_{j_0+j'} - \sum_{j'\neq 0}^{J} \delta_{j_0}^{(1)} \sigma_{j_0+j'}, \tag{34b}$$

respectively. Since the left hand sides of (34a) and (34b) are equal to $1 - a_{j_0,0}$ and $1 - c_{j_0,0}$ from (31), respectively, we can write the equations that determine $a_{j_0,0}$ and $c_{j_0,0}$ as

$$a_{j_0,0} = \frac{\sigma_{j_0}}{\sum_{j'=0}^{J} \sigma_{j_0+j'}} \left[ 1 - \frac{1}{H\Delta t} \sum_{j'\neq 0}^{J} h_{j_0}^{(1)} \sigma_{j_0+j'} \right] \tag{35a}$$

and

$$c_{j_0,0} = \frac{\sigma_{j_0}}{\sum_{j'=0}^{J} \sigma_{j_0+j'}} \left[ 1 + \sum_{j'\neq 0}^{J} \delta_{j_0}^{(1)} \sigma_{j_0+j'} \right], \tag{35b}$$

respectively. Then the coefficients $a_{j_0,j'}$ and $c_{j_0,j'}$ can be obtained from (33a) and (33b), respectively.

For a square grid, the numerical procedure described above produces coefficients virtually identical to those shown in Tables 2 and 3, which have been obtained with the analytical method. For a more general grid, the procedure must be repeated for all possible $j_0$ unless we can take advantage of geometrical symmetry that may exist in the grid. The choice of the minimum J's should be made requiring that the scheme be stable. For a quasi-regular grid such as a geodesic grid, the choice can be guided by the stability for a similar regular grid such as the hexagonal grid, whereas it must be done empirically for a fully irregular grid.

For comparison purposes, we performed numerical integrations of linearized shallow water equations using explicit schemes with small time steps, the implicit trapezoidal (TZ) and TETZ schemes with different Courant numbers. The explicit integration uses a two-level forward-backward time-integration scheme with a second-order centered special differencing. The implicit TZ scheme is given by (29a) and (29b) with a second-order centered Laplacian. In solving (29a), we used an iteration method. The coefficients of the TETZ scheme are obtained by the procedure described by (29) to (30) on a Cartesian grid using J's for the given Courant numbers tabulated in the lower row of Table 1. The explicit, TZ and TETZ models described above are applied to simulation of gravity-wave propagations on a square grid (100 km grid distance in both directions) in a square domain (200 grid points in both directions) with cyclic boundary conditions. The initial surface height consists of a uniform component of 10 km deep and a cone-shaped perturbation with a 100m high maximum centered at the middle of the domain. Fig. 6 shows the surface height perturbation at t=320 mins obtained by the explicit with a small time step, the implicit TZ and TETZ schemes for the Courant

numbers, 1, 3 and 10. The simulations with the TZ and TETZ schemes are virtually identical and both show reasonable propagation speed but dispersion and dissipation errors increasing with the Courant number. This type of errors is expected for the large Courant numbers with an implicit and the mimicking MED schemes, which should be selected for their superior stability characteristics rather than the accuracy they provide.

We also quantitatively studied the errors of the simulated surface height by calculating the root-mean-square (RMS) error between the solutions with the TZ and TETZ schemes obtained by various horizontal grid distances, namely 12.5km, 25km, 50 km, 100km and 200km, and a reference solution for the fixed Courant numbers 3 and 5. The TZ solution with 12.5km grid distance for the respective Courant number is selected as the reference solution. The simulations use the same initial condition discussed in the previous paragraph and the model is integrated for 80 mins. Since the solutions are virtually axi-symmetric, we analyzed the one-dimensional surface height data on a row at the middle of the domain. Interpolations from lower horizontal resolutions to the reference resolution is made through a running fifth-order polynomial fit using information from six grid points. In Fig. 7, the resulting RMS errors are displayed as functions of the grid distance in a log-log diagram for two Courant numbers. The figure shows that the RMS errors with the TZ and TETZ schemes are virtually identical and the slope of the line connecting the scattered points indicates approximately a second-order error convergence in time and space.

## 6. Application of the MED to the nonlinear shallow-water equations on a square grid and numerical simulations of surface waves

To demonstrate the performance of the MED scheme on a square grid, we have constructed a nonlinear 2-D shallow-water model based on the ETZ and TETZ schemes using

the coefficients $a_{i',j'}$ and $c_{i',j'}$ obtained through the procedure described in section 4. For the tests we present here, we assume that the fluid depth is quasi-uniform, there is no Coriolis force, and the fluid is at rest initially. The MED scheme for the nonlinear shallow-water equations can be written as

$$h_{i,j}^{(n+1)} = \mathbf{C}\left[h^{(n)}\right]_{i,j} - H\Delta t\mathbf{A}\left[\delta^{(n)}\right]_{i,j} - \Delta t\tilde{\nabla}\cdot\left[\left(h^{(*)} - H\right)\cdot\mathbf{v}_{\chi}^{(*)}\right]_{i,j} \qquad (36a)$$

and

$$\delta_{i,j}^{(n+1)} = \mathbf{C}\left[\delta^{(n)}\right]_{i,j} - g\Delta t\mathbf{A}\left[\tilde{\nabla}^2 h^{(n)}\right]_{i,j} - \Delta t\left[\tilde{\nabla}^2 K^{(*)}\right]_{i,j}, \qquad (36b)$$

where the superscript (*) denotes a provisional value at time level (n+1), $\mathbf{v}_{\chi}$ is the divergent component of the velocity, and K is the kinetic energy $\frac{1}{2}\mathbf{v}_{\chi}^2$. The predictor we used to determine $h^{(*)}$, $\mathbf{v}_{\chi}^{(*)}$ and $K^{(*)}$ is described in Appendix.

The model is used to simulate propagation of waves with different values of the Courant number. The model domain is a 30,000 km by 30,000 km square with cyclic or rigid lateral boundaries. The horizontal grid size is $\Delta x = \Delta y = 100$ km. There is no topography at the lower boundary. The initial height of the free surface consists of a uniform height H (=10 km) and a cone-shaped perturbation field with a maximum height of 100 m. The fluid is initially at rest. The time step is determined from the specified value of the Courant number by using $c \approx 313$ m/s and the grid size; for example, $\Delta t = 319$ sec and $\Delta t = 1595$ sec for $\mu = 1$ and $\mu = 5$, respectively.

*a. Simulations with cyclic boundaries*

In these simulations, the coefficients given in Tables 2 and 3 are used. The initial height of the free surface for these simulations is shown in Fig. 8. The snapshots of simulated waves are shown in Fig. 9 at t = 7 h, 14 h, 20 h and 27 h from the initial for the Courant numbers 1, 3, 5 and 10 with corresponding J's 3, 7, 12 and 24. These results show propagation of waves as expected from the initial location of the perturbation. The solution is stable and close to neutral for all Courant numbers. The simulations with very large J's (not shown), for which the scheme becomes the ETZ scheme, are virtually identical to those shown in Fig. 9, demonstrating that solutions with the TETZ scheme are close approximations to those with the implicit trapezoidal scheme.

*b. Simulations with rigid boundaries*

For a domain with cyclic boundaries such as the one used in the previous subsection, the scheme has an identical form at all grid points. For a rectangular or irregularly shaped domain with rigid boundaries, however, the coefficients in the scheme vary, especially at grid points close to the boundaries. For such a domain, we calculate the coefficients using the numerical method described in section 5 ignoring contributions from the grid points outside of the domain. The algorithm then automatically adjusts the coefficients on the inner grid points.

To demonstrate the performance of the TETZ scheme with rigid boundaries, we perform two simulations, first of which is similar to those presented in subsection 6*a* but with the initial perturbation placed off-center in the domain. The snapshots of simulated waves are shown in Fig. 10 at t = 7 h, 14 h, 20 h and 27 h from the initial for Courant numbers 3 and 5 with corresponding J's 7 and 12. These results show propagation of waves as expected from the initial location of the perturbation with reflections at the boundaries. The second

simulation we present here uses an irregularly-shaped domain with rigid boundaries. The initial condition and the domain are shown in Fig. 11, in which the green patches indicate Land. The snapshots of simulated waves are shown in Fig. 12 at t = 4 h, 8 h, 12 h and 16 h from the initial for Courant numbers 3 and 5 with corresponding J's 7 and 12. These results show no computational difficulties due to the irregular boundary.

**7. Summary and conclusions**

The purpose of this study is to seek the feasibility of constructing an explicit scheme that does essentially the same job as an implicit scheme with a finite number of grid points in space. In this paper, we have selected the trapezoidal (TZ) scheme as the target implicit scheme to be mimicked. A family of multi-point explicit differencing (MED) schemes has been introduced to do the job.

To illustrate how a truncated equivalent trapezoidal (TETZ) scheme as a member of the MED family can be constructed, we first considered the case of a rectangular grid with cyclic boundary conditions, for which the coefficients in the scheme can be analytically determined. We then presented a numerical method to construct such a scheme applicable to any grid with arbitrary boundary conditions including irregular rigid boundaries. The results of the analytical method for the square grid were used to verify the numerical method. Performance of the TETZ scheme with the nonlinear shallow-water equations was demonstrated with cyclic and irregular rigid boundaries. These results show that the TETZ scheme can produce stable and near-neutral solutions even when the Courant number is much larger than unity.

The issue we have addressed in this paper is how to construct a non-global scheme that is applicable over a wide range of the Courant number. We do not necessarily claim that

the scheme presented here is more economical than usual explicit schemes with smaller time steps or any particular semi-implicit scheme. In a MED scheme, the number of grid points necessary to maintain stability and, therefore, the CPU time needed for each time step increase as the Courant number increases. The overall economy of a MED scheme, however, depends on many other factors, such as the code structure for parallel computing and the sophistication of model dynamics and physics. We do claim, however, that with a MED scheme the Courant number for the fast moving waves does not limit the stability of a model. This is advantageous for complex multi-level models with detailed physics, in which the fraction of the overhead due to the use of multiple-points in a MED scheme can be negligibly small. It is shown that the MED approach can easily be applied to arbitrary grids with irregular boundaries, and does not require information from all the grid points in the domain.

In this paper, we assumed that the height of the free surface is quasi-uniform and the amplitude of the disturbance is sufficiently smaller than the mean height. This allowed us to use the linearized system to determine the coefficients in the TETZ scheme. Although the performance of the system was tested with the nonlinear system, the initial conditions were chosen in such a way that the system is quasi-linear. We are currently working on generalization of the approach so that it can also be applied to the models with highly varying layer thickness. This is the case, for example, with the hybrid isentropic-sigma vertical coordinate model of Konor and Arakawa (1997). We are also working on implementation of this approach in 3D atmospheric models, applying multi-point averaging to those terms that would vanish if the anelastic approximation were used in the model. In this way, the model can be made stable for large Courant numbers with respect to acoustic waves, leaving anelastic motions unaffected.

In principle, the MED approach can be applied to any implicit or partially implicit scheme other than the implicit trapezoidal scheme. Also, we may be able to rewrite the MED scheme as a multi-step iterative scheme with fewer grid points in space. If this is possible, it brings more flexibility to the MED method by introducing a choice between the multiple steps with fewer spatial grid points and fewer steps with more spatial grid points without changing the stability property of the solutions. In practical applications, the choice between these and any hybrid approaches can be made to maximize the computational efficiency for the specific computer architecture.

The MED approach can also be applied to the advection equation. We are working on the construction of a family of MED schemes that are stable for a wide range of the Courant number for advection while using an Eulerian approach.

*Acknowledgements*. We thank Professor David Randall for his encouragement and support of this work. Dr. Ross Heikes' help in plotting some of the figures is greatly appreciated. We also thank two anonymous reviewers for their constructive comments and suggestions. This work was funded by U.S. DOE under grant numbers DE-FG02-04ER63848, DE-FG02-02ER63370 and DE-FC02-06ER64302 to Colorado State University, CSU Contracts G-3816-3 and G-3818-1 to UCLA, and NSF under grant number ATM-0415184 to Colorado State University.

## Appendix

### The predictor used in the nonlinear terms of the shallow-water model

We predict h for time level (n+1) by the forward scheme using

$$h_{i,j}^{(\dagger)} = h_{i,j}^{(n)} - \Delta t \left\{ \tilde{\nabla} \cdot \left[ \left( h^{(n)} - H \right) \mathbf{v}_{\chi}^{(n)} \right] \right\}_{i,j}, \tag{A1}$$

where the components of $\mathbf{v}_{\chi}$ are obtained by

$$\left[ u_{\chi}^{(n)} \right]_{i+1/2,j} = \frac{1}{\Delta x} \left[ \chi_{i+1,j}^{(n)} - \chi_{i,j}^{(n)} \right] \tag{A2a}$$

and

$$\left[ v_{\chi}^{(n)} \right]_{i,j+1/2} = \frac{1}{\Delta y} \left[ \chi_{i,j+1}^{(n)} - \chi_{i,j}^{(n)} \right] \tag{A2b}$$

at the half-integer grid points shown in Fig. 2. The velocity potential $\chi$ in (A2a) and (A2b) is obtained by solving

$$\left[ \tilde{\nabla}^2 \chi^{(n)} \right]_{i,j} \equiv \delta_{i,j}^{(n)} \tag{A3}$$

in the domain with proper boundary conditions. A second-order centered finite-differencing is used in the discretization of the divergence $\tilde{\nabla}$ and Laplacian $\tilde{\nabla}^2$. The kinetic energy at the point (i , j) is defined by

$$K_{i,j}^{(n)} = \frac{1}{2}\left\{\frac{1}{2}\left[u_\chi^{(n)}\right]_{i+1/2,j}^2 + \frac{1}{2}\left[u_\chi^{(n)}\right]_{i-1/2,j}^2\right\} + \frac{1}{2}\left\{\frac{1}{2}\left[v_\chi^{(n)}\right]_{i,j+1/2}^2 + \frac{1}{2}\left[v_\chi^{(n)}\right]_{i,j-1/2}^2\right\}. \quad \text{(A4)}$$

Using (A4), we predict the divergence by

$$\delta_{i,j}^{(*)} = \delta_{i,j}^{(n)} - \Delta t\left[\tilde{\nabla}^2 K^{(n)}\right]_{i,j}. \quad \text{(A5)}$$

Then, from $\left[\tilde{\nabla}^2\chi^{(*)}\right]_{i,j} = \delta_{i,j}^{(*)}$ and following the same procedure given by (A2a), (A2b) and (A4), we find $\mathbf{v}_\chi^{(*)}$ and $K^{(*)}$. To find $h^{(*)}$, we use

$$h_{i,j}^{(*)} = h_{i,j}^{(n)} - \Delta t\left\{\tilde{\nabla}\cdot\left[\left(h^{(\dagger)} - H\right)\mathbf{v}_\chi^{(*)}\right]\right\}_{i,j}, \quad \text{(A6)}$$

where $h^{(\dagger)}$ is obtained from (A1). $\mathbf{v}_\chi^{(*)}$, $K^{(*)}$ and $h^{(*)}$ are used in (36a) and (36b).

## References


Bourke, W., 1974: A Multi-Level Spectral Model. I. Formulation and Hemispheric Integrations. *Mon. Wea. Rev.*, **102**, 687-701.

Brandt, A., 1977: Multi-level adaptive solutions to boundary value problems. *Math. Comp.*, **31**, 333-390.

Briggs, W. L., V. E. Henson and F. McCormick, 2000: A multigrid tutorial. Second Edition. *SIAM*. 193pp.

Burridge, D. M., 1975: A split semi-implicit reformulation of the Bushby-Timpson 10-level model. *Quart. J. Roy. Meteor. Soc.,* **101**, 777-792.

Cullen, J. P., 1990: A test of a semi-implicit integration technique for a fully compressible non-hydrostatic model. *Quart. J. Roy. Meteor. Soc.,* **116**, 1253-1258.

Eriksson, C., C. Johnson and A. Logg, 2003: Explicit time stepping for stiff ODE's. *SIAM J. Sci. Comp.*, **25**, 1142-1157.

Frank, J., S. Reich, A. Staniforth, A. White and N. Wood, 2005: Analysis of a regularized, time-staggered method and its link to the semi-implicit method. *Atm. Sci. Letters*, **6**, 97-104.

Fulton, S. R., P. E. Ciesielski and W. Schubert, 1986: Multi-grid methods for elliptic problems: A review. *Mon. Wea. Rev.*, **114**, 943-959.

Holton, J. R., 1967: A stable finite difference scheme for the linearized vorticity and divergence equation system. *J. Appl. Meteor.*, **6**, 519-522.

Israeli, M., N. H. Naik and M. A. Cane, 2000: An unconditionally stable scheme for the shallow water equations. *Mon. Wea. Rev.*, **128**, 810-823.

Konor, C. S., and A. Arakawa, 1997: Design of an atmospheric model based on a generalized vertical coordinate. *Mon. Wea. Rev.*, **125**, 1649-1673.

Kurihara, Y., 1965: On the use of implicit and iterative methods for the time integration of the wave equation. *Mon. Wea. Rev.*, **93**, 33-46.

Kwizak, M and A. J. Robert, 1971: A Semi-implicit scheme for grid point atmospheric models

of the primitive equations. *Mon. Wea. Rev.*, **99**, 32-36.

Purser, R. J., and L. M. Leslie, 1994: An efficient semi-Lagrangian scheme using third-order semi-implicit time integration and forward trajectories. . *Mon. Wea. Rev.*, **122** 745-756.

Robert, A, J. Henderson and C. Turnbull, 1972: An implicit time integration scheme for baroclinic models of the atmosphere. *Mon. Wea. Rev.*, **100**, 329-334.

Simmons, A.J., B. J. Hoskins, D. M. Burridge, 1978: Stability of the Semi-Implicit Method of Time Integration. *Mon. Wea. Rev.*, **106**, 405-412.

Tanguay, M., A. Robert, and R. Laprise, 1990: A Semi-implicit Send-Lagrangian Fully Compressible Regional Forecast Model. *Mon. Wea. Rev.*, **119** 1970-1980.

Tapp, M., and P. W. White, 1976: A non-hydrostatic mesoscale model. *Quart. J. Roy. Meteor. Soc.,* **102**, 277-296.

Verwer, J. G., 1996: Explicit Runge-Kutta method for parabolic partial differential equations. *Appl. Num. Math.*, **22** 359-379.

Yeh, K-S, J. Côté, S. Gravel, A. Méthot, A. Patoine, M. Roch and A. Staniforth, 2002: The CMC–MRB Global Environmental Multiscale (GEM) Model. Part III: Nonhydrostatic Formulation. *Mon. Wea. Rev.*, **130** 339-356.

**Figure Captions**

Fig. 1. See text for explanation.

Fig. 2. Portion of the grid used in the discretizations.

Fig. 3. Coefficients $a_{i',0}$ and $c_{i',0}$ as a function of i′ for selected Courant numbers with a sufficiently large J. Coefficients only for $-5 \le i' \le 5$ are shown.

Fig. 4. Maximum of $\left(8\mu^{*}\tilde{G}_{T}\right)^{2}$ in the interval of $-\pi \le \xi \le \pi$ and $-\pi \le \eta \le \pi$ as a function of J.

Fig. 5. Selected cells of an arbitrary grid.

Fig. 6. 1D-section of surface height perturbation of a two-dimensionally propagating wave at t=320 mins obtained by an explicit, trapezoidal implicit (TZ) and the TETZ schemes for different Courant numbers. Figure shows half of the domain from the domain center indicated by grid point 0 to the boundary of the domain. Simulation starts from a cone-shaped initial perturbation at the center of the domain. Arrows indicate the propagation direction.

Fig. 7. Root-mean-square (RMS) errors for different spatial and temporal resolutions for selected Courant numbers. Squares and circles represent solutions of the TZ and TETZ schemes, respectively. The slope of the dashed line represents second-order convergence.

Fig. 8. Initial free surface height perturbation placed at the center of the domain used in the simulations with the cyclic boundaries.

Fig. 9. Time evolution of the free surface height simulated with the cyclic boundaries by using the Courant numbers $\mu = 1$, 3, 5 and 10 and corresponding J = 3, 7, 12 and 24, respectively.

Fig. 10. Time evolution of the free surface height simulated with the rigid boundaries by using the Courant numbers $\mu = 3$ and 5 and corresponding J = 7 and 12, respectively.

Fig. 11. Initial free surface height perturbation used in the simulations with an irregular rigid boundary. Green patches indicate Land.

Fig. 12. Same as Fig. 8 but for a domain with an arbitrarily-shaped rigid boundary. Green patches indicate Land.

**Table captions**

Table 1. Minimum J's that maintain $\left(8\mu^{*}\tilde{G}_{T}\right)^{2}_{max}$ under 1.05 (upper row) and 1.01 (lower row).

Table 2. Truncated coefficients $\tilde{a}_{i',j'}$ for selected Courant numbers and corresponding J's.

Table 3. Same as Table 2 but for $\tilde{c}_{i',j'}$.

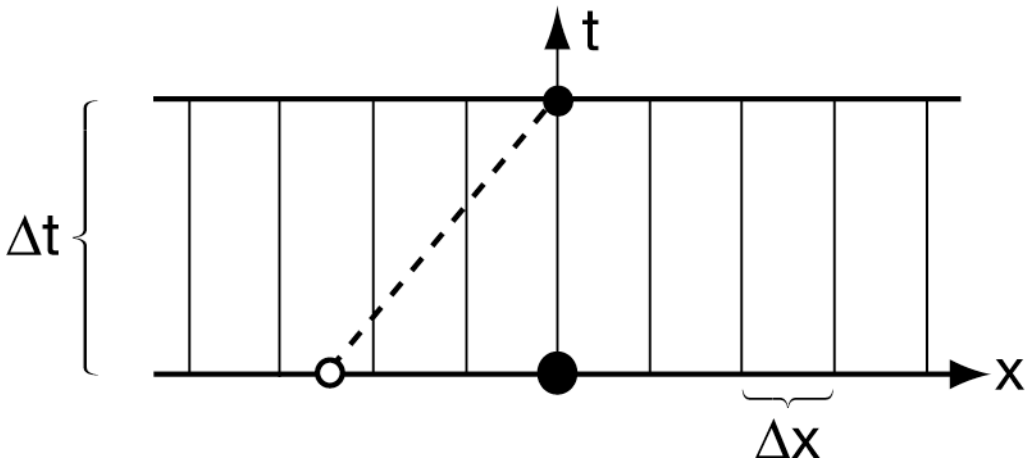


Fig. 1. See text for explanation.

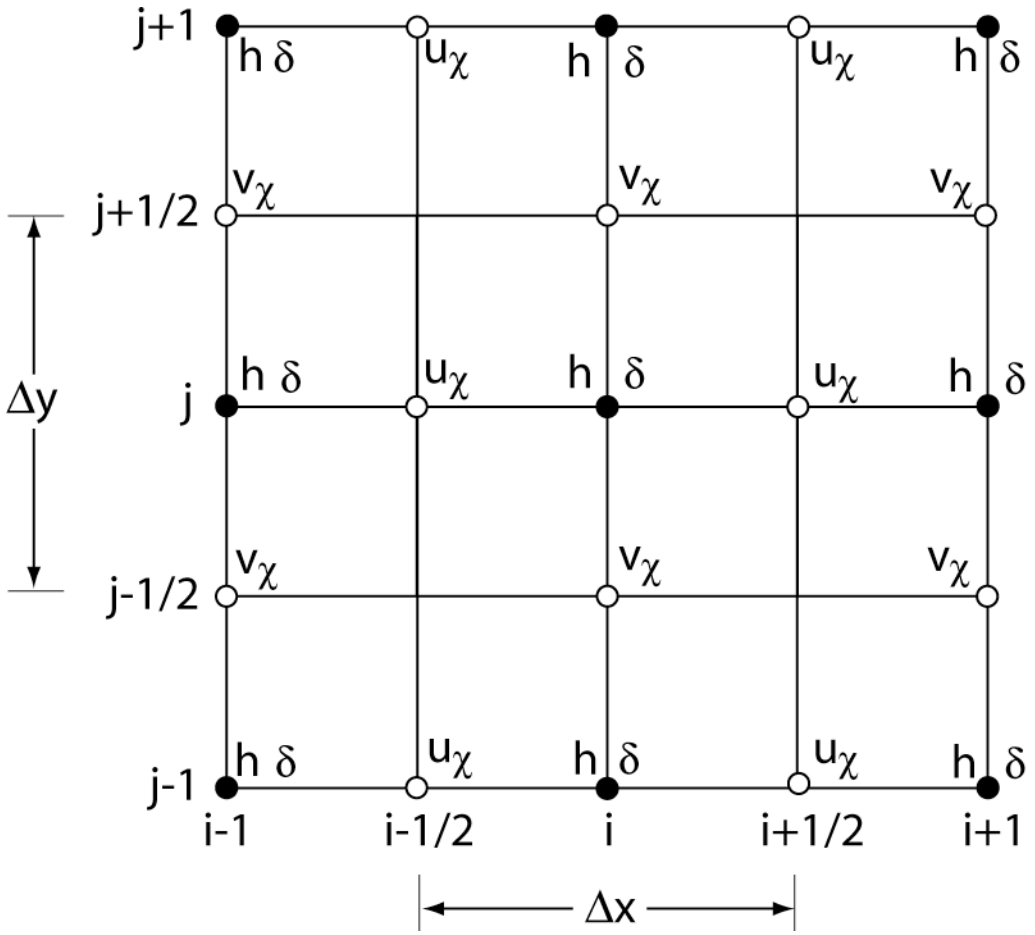


Fig. 2. Portion of the grid used in the discretizations.

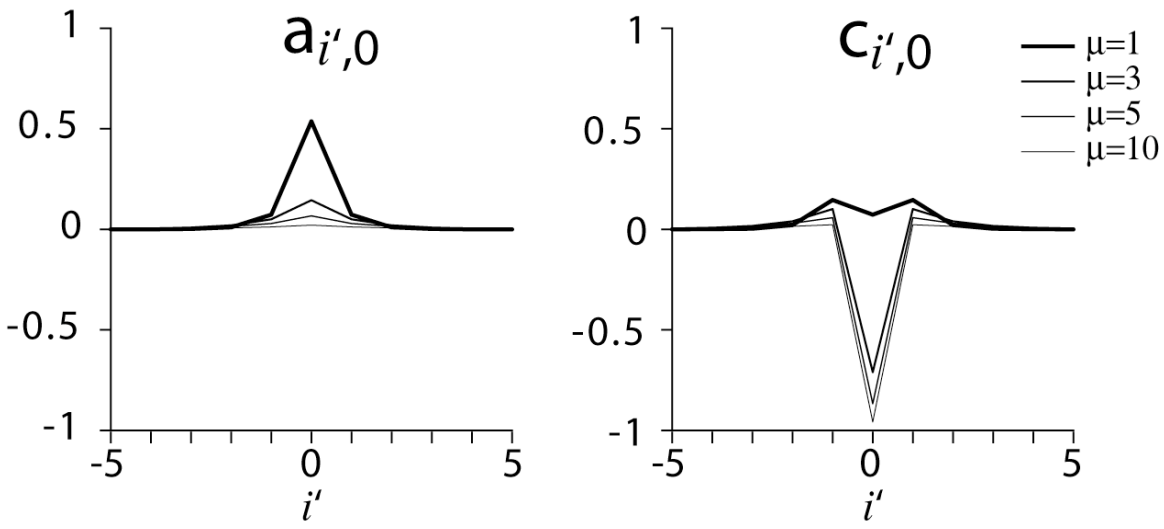


Fig. 3. Coefficients $a_{i',0}$ and $c_{i',0}$ as a function of i′ for selected Courant numbers with a sufficiently large J. Coefficients only for $-5 \le i' \le 5$ are shown.

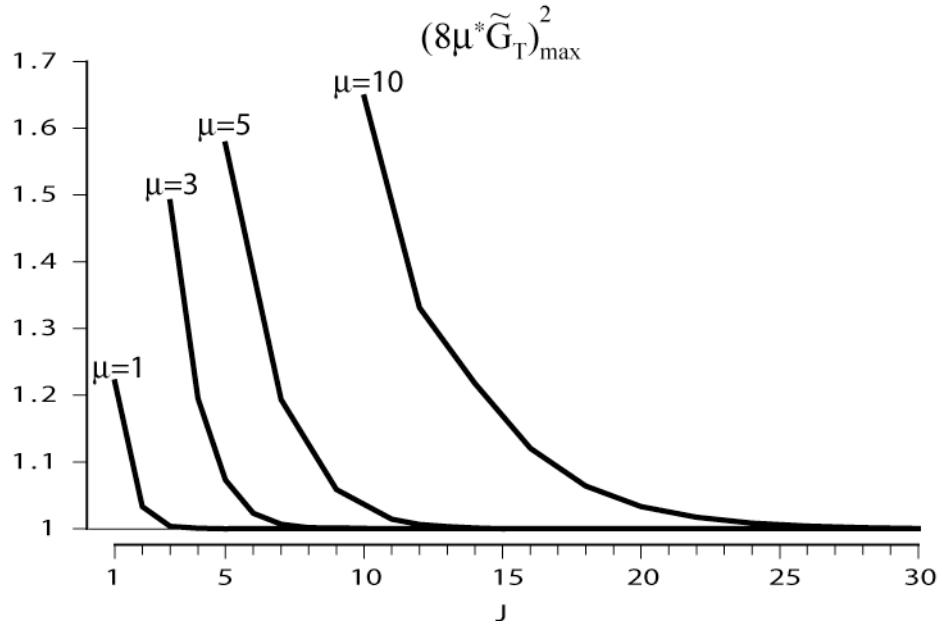


Fig. 4. Maximum of $\left(8\mu^*\tilde{G}_T\right)^2$ in the interval of $-\pi \le \xi \le \pi$ and $-\pi \le \eta \le \pi$ as a function of J.

| | $\mu$ | 1 | 2 | 3 | 4 | 5 | 6 | 7 | 8 | 9 | 10 |
|---|---|---|---|---|---|---|---|---|---|---|---|
| J | $(8\mu^{*}\widetilde{G}_T)^2_{max} \le 1.05$ | **2** | **4** | **6** | **8** | **10** | **12** | **13** | **15** | **18** | **20** |
| | $(8\mu^{*}\widetilde{G}_T)^2_{max} \le 1.01$ | **3** | **5** | **7** | **9** | **12** | **14** | **16** | **19** | **21** | **24** |

Table 1. Minimum J's that maintain $\left(8\mu^{*}\tilde{G}_T\right)^2_{max}$ under 1.05 (upper row) and 1.01 (lower row).

$\mu$=1 J=3

| | | | | |
|---|---|---|---|---|
| 3 | .0016 | .0008 | .0003 | .0001 |
| 2 | .0104 | .0040 | .0011 | .0003 |
| 1 | .0732 | .0193 | .0040 | .0008 |
| 0 | .5367 | .0732 | .0104 | .0016 |
| j´ / i´ | 0 | 1 | 2 | 3 |

$\mu$=3 J=7

| | | | | | | |
|---|---|---|---|---|---|---|
| 5 | .0018 | .0017 | .0013 | .0009 | .0006 | .0004 |
| 4 | .0039 | .0034 | .0025 | .0017 | .0010 | .0006 |
| 3 | .0085 | .0070 | .0048 | .0029 | .0017 | .0009 |
| 2 | .0198 | .0146 | .0087 | .0048 | .0025 | .0013 |
| 1 | .0503 | .0292 | .0146 | .0070 | .0034 | .0017 |
| 0 | .1452 | .0503 | .0198 | .0085 | .0039 | .0018 |
| j´ / i´ | 0 | 1 | 2 | 3 | 4 | 5 |

$\mu$=5 J=12

| | | | | | | |
|---|---|---|---|---|---|---|
| 5 | .0030 | .0028 | .0024 | .0019 | .0015 | .0011 |
| 4 | .0049 | .0045 | .0037 | .0029 | .0021 | .0015 |
| 3 | .0083 | .0074 | .0057 | .0041 | .0029 | .0019 |
| 2 | .0148 | .0122 | .0086 | .0057 | .0037 | .0024 |
| 1 | .0291 | .0198 | .0122 | .0074 | .0045 | .0028 |
| 0 | .0664 | .0291 | .0148 | .0083 | .0049 | .0030 |
| j´ / i´ | 0 | 1 | 2 | 3 | 4 | 5 |

$\mu$=10 J=24

| | | | | | | |
|---|---|---|---|---|---|---|
| 5 | .0027 | .0026 | .0024 | .0021 | .0018 | .0015 |
| 4 | .0036 | .0035 | .0031 | .0027 | .0022 | .0018 |
| 3 | .0050 | .0047 | .0040 | .0033 | .0027 | .0021 |
| 2 | .0072 | .0064 | .0052 | .0040 | .0031 | .0024 |
| 1 | .0114 | .0088 | .0064 | .0047 | .0035 | .0026 |
| 0 | .0212 | .0114 | .0072 | .0050 | .0036 | .0027 |
| j´ / i´ | 0 | 1 | 2 | 3 | 4 | 5 |

Table 2. Truncated coefficients $\tilde{a}_{i',j'}$ for selected Courant numbers and corresponding J's.

μ=1 J=3

| i′ \ j′ | 0 | 1 | 2 | 3 |
|---|---|---|---|---|
| 3 | .0024 | .0019 | .0003 | -.0006 |
| 2 | .0191 | .0086 | .0021 | .0003 |
| 1 | .1466 | .0412 | .0086 | .0019 |
| 0 | .0710 | .1466 | .0191 | .0024 |

μ=3 J=7

| i′ \ j′ | 0 | 1 | 2 | 3 | 4 | 5 |
|---|---|---|---|---|---|---|
| 5 | .0039 | .0035 | .0028 | .0019 | .0012 | .0008 |
| 4 | .0077 | .0068 | .0050 | .0033 | .0020 | .0012 |
| 3 | .0168 | .0138 | .0093 | .0057 | .0033 | .0019 |
| 2 | .0392 | .0287 | .0171 | .0093 | .0050 | .0028 |
| 1 | .1000 | .0579 | .0287 | .0138 | .0068 | .0035 |
| 0 | -.7100 | .1000 | .0392 | .0168 | .0077 | .0039 |

μ=5 J=12

| i′ \ j′ | 0 | 1 | 2 | 3 | 4 | 5 |
|---|---|---|---|---|---|---|
| 5 | .0059 | .0055 | .0047 | .0038 | .0029 | .0021 |
| 4 | .0097 | .0089 | .0074 | .0056 | .0041 | .0029 |
| 3 | .0165 | .0147 | .0114 | .0082 | .0056 | .0038 |
| 2 | .0295 | .0242 | .0171 | .0114 | .0074 | .0047 |
| 1 | .0580 | .0395 | .0242 | .0147 | .0089 | .0055 |
| 0 | -.8673 | .0580 | .0295 | .0165 | .0097 | .0059 |

μ=10 J=24

| i′ \ j′ | 0 | 1 | 2 | 3 | 4 | 5 |
|---|---|---|---|---|---|---|
| 5 | .0053 | .0051 | .0047 | .0041 | .0035 | .0030 |
| 4 | .0072 | .0069 | .0061 | .0052 | .0043 | .0035 |
| 3 | .0099 | .0093 | .0080 | .0065 | .0052 | .0041 |
| 2 | .0144 | .0127 | .0102 | .0080 | .0061 | .0047 |
| 1 | .0227 | .0175 | .0127 | .0093 | .0069 | .0051 |
| 0 | -.9577 | .0227 | .0144 | .0099 | .0072 | .0053 |

Table 3. Same as Table 2 but for $\tilde{c}_{i',j'}$.

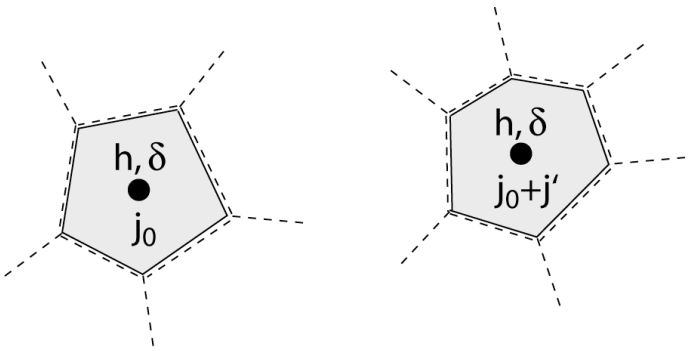


Fig. 5. Selected cells of an arbitrarily-shaped grid.

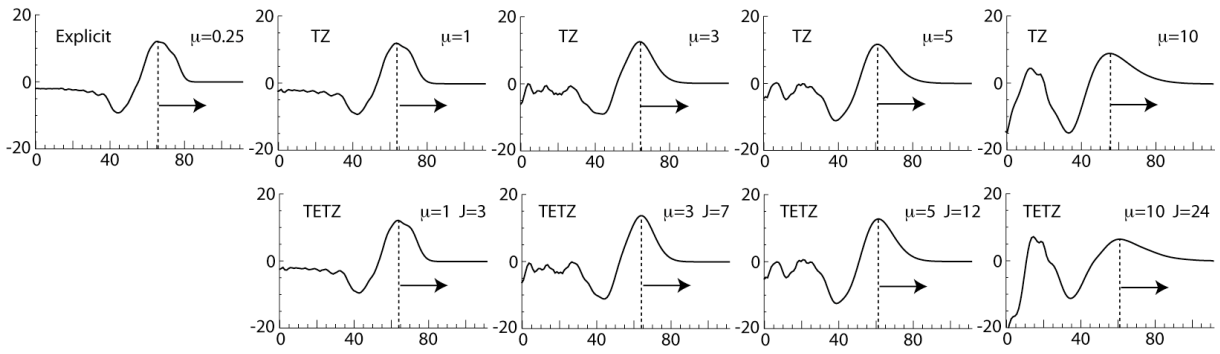


Fig. 6. 1D-section of surface height perturbation of a two-dimensionally propagating wave at t=320 mins obtained by an explicit, trapezoidal implicit (TZ) and the TETZ schemes for different Courant numbers. Figure shows half of the domain from the domain center indicated by grid point 0 to the boundary of the domain. Simulation starts from a cone-shaped initial perturbation at the center of the domain. Arrows indicate the propagation direction.

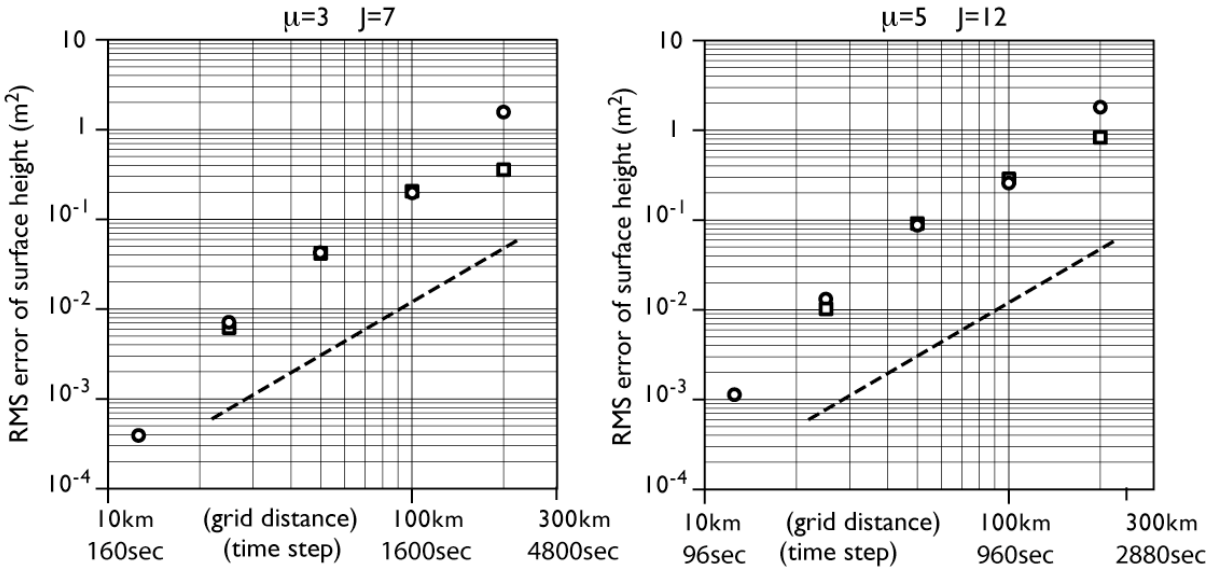


Fig. 7. Root-mean-square (RMS) errors for different spatial and temporal resolutions for selected Courant numbers. Squares and circles represent solutions of the TZ and TETZ schemes, respectively. The slope of the dashed line represents second-order convergence.

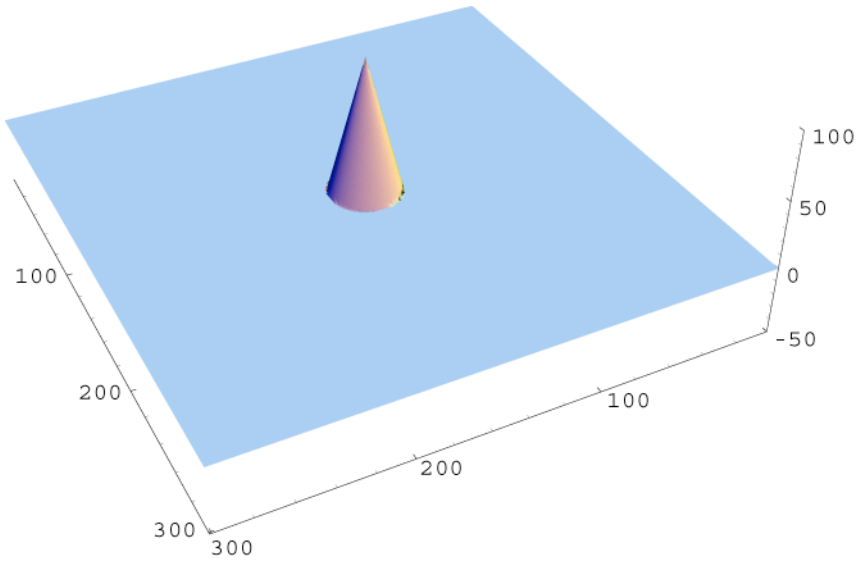


Fig. 8. Initial free surface height perturbation placed at the center of the domain used in the simulations with the cyclic boundaries.

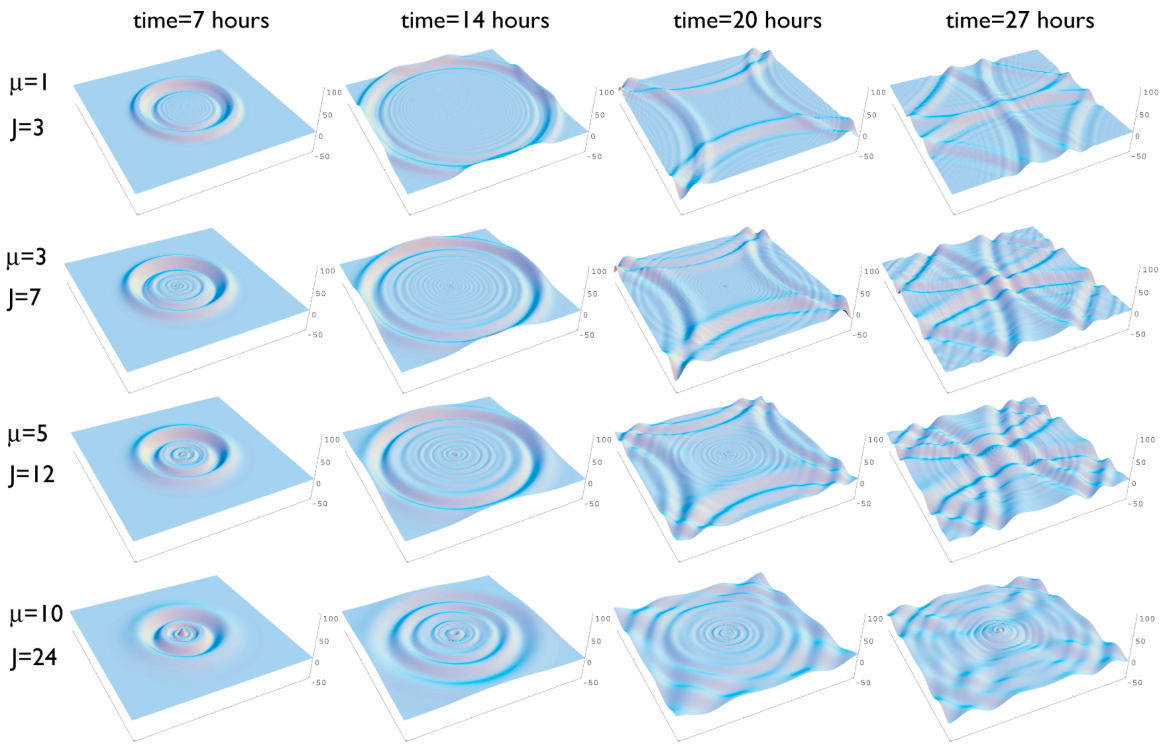


Fig. 9. Time evolution of the free surface height simulated with the cyclic boundaries by using the Courant numbers $\mu = 1$, 3, 5 and 10 and corresponding J = 3, 7, 12 and 24, respectively.

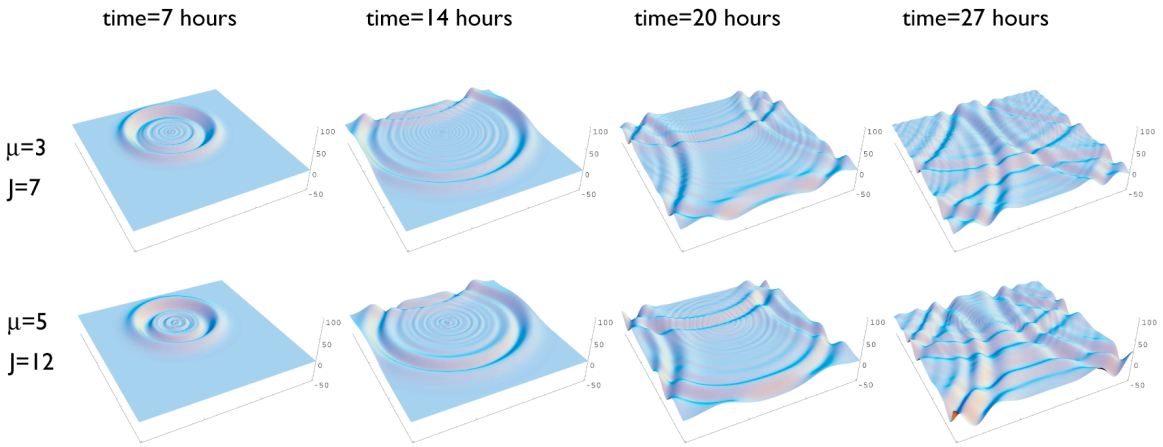


Fig. 10. Time evolution of the free surface height simulated with a rigid boundary in a square domain by using the Courant numbers $\mu = 3$ and 5 and corresponding J = 7 and 12, respectively.

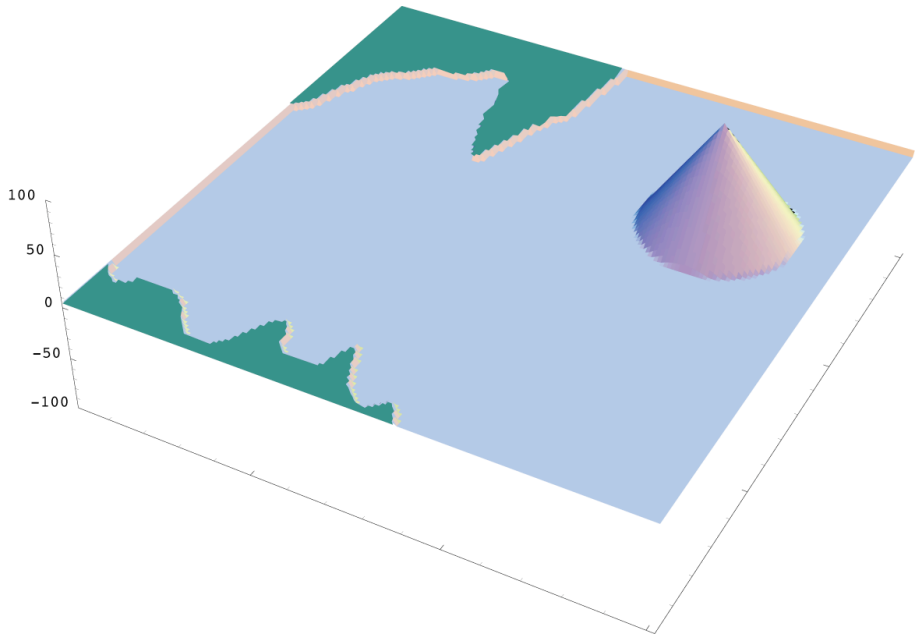


Fig. 11. Initial free surface height perturbation used in the simulations with an arbitrarily-shaped rigid boundary. Green patches indicate Land.

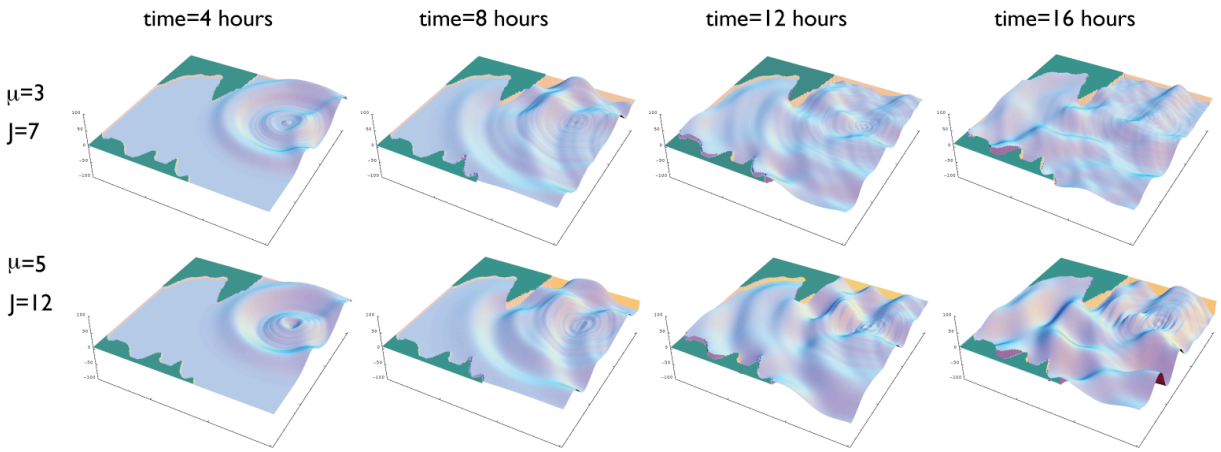


Fig. 12. Same as Fig. 8 but for a domain with an arbitrarily-shaped rigid boundary. Green patches indicate Land.